Asia-Pacific Journal of Atmospheric Sciences
https://doi.org/10.1007/s13143-022-00304-2

Online ISSN 1976-7951
Print ISSN 1976-7633

ORIGINAL ARTICLE

A Comparative Assessment of Changes in Heat-Related Mortality Risk Under the RCP2.6 and RCP8.5 Scenarios Based on the CORDEX-CORE Ensembles

Yuwen Fan[1] · **Eun-Soon Im**[1,2]

Received: 30 May 2022 / Revised: 18 October 2022 / Accepted: 16 November 2022

Abstract
This study assesses the future heat-related mortality risk under varying levels of warming specified by the RCP2.6 and RCP8.5 scenarios using dynamically downscaled ensemble projections across six different domains. The excess mortality risk due to heat is estimated by the empirical relationship between daily maximum temperature (Tmax) and mortality. The changes in heat-related mortality based on three empirical formulas derived from different countries' data are compared to examine the sensitivity of change patterns to the empirical formula. The ensemble projections reveal a drastic increase in heat-related mortality risk under the RCP8.5 scenario. However, a significant reduction is expected by limiting greenhouse gas emissions to the RCP2.6 level. While mitigation's possible benefit is clearly exemplified by comparing the mortality risk derived from RCP2.6 and RCP8.5 projections, this study also provides valuable insights into regional hotspots by comparing the results from multi-domains. Regardless of the emission scenario (RCP2.6 vs. RCP8.5) and empirical formulas that represent the relationship between temperature and mortality, the most vulnerable regions to heat-related mortality risk are identified in the low-latitude near the equator where the adaptation capacities to avoid serious consequences are found to be poor. The higher risk of heat-related mortality in the future is largely attributable to a significant increase in frequency exceeding the optimum temperature where the mortality risk is minimum during the historical period.

Keywords Heat-related mortality risk · CORDEX-CORE ensemble simulations · Mitigation impact · Empirical relationship between temperature and mortality

1 Introduction

As more intense and frequent hot extremes have been witnessed in the recent past (Vogel et al. 2019; Saeed et al. 2021; Im et al. 2019), the continued repetition of record-breaking hot extremes is projected in the future, in alignment with increased greenhouse gas (GHG) concentrations (Intergovernmental Panel on Climate Change 2014; Sylla et al. 2018). One of the most direct adverse impacts expected from sweltering temperatures will be the surge in heat-related mortality (Anderson and Bell 2011; Guo et al. 2018). It is widely accepted that escalating temperatures can lead to excess death directly. Moreover, the accumulated heat stress may trigger the onset of other serious diseases, such as cardiovascular or respiratory diseases (Guo et al. 2018), which does not rule out the possibility of death as the indirect repercussion of extreme heat events. However, despite intuitively reasonable linkage, an unambiguous assessment of heat-related mortality and the generalization of the association between temperature and mortality is not necessarily straightforward (Chen et al. 2018). In addition to the lack of robust methodological approaches to estimate heat-related excess mortality, the reliability of data quality related to the categorization of deaths is also predicated on the target regions' socioeconomic status (Intergovernmental Panel on Climate Change 2012). Not to mention, it is much more challenging to assess the future projections of heat-related mortality in a changing climate,

Responsible Editor: Maeng-Ki Kim

✉ Eun-Soon Im
ceim@ust.hk

[1] Division of Environment and Sustainability, The Hong Kong University of Science and Technology, Hong Kong, China

[2] Department of Civil and Environmental Engineering, The Hong Kong University of Science and Technology, Academic Building 4602, Clear Water Bay, Kowloon, Hong Kong, China

Published online: 05 December 2022

due to the unavoidable uncertainties stemming from future climate information as well as evolving heat acclimatization that can affect the empirical relationship between temperature and mortality.

To estimate the heat-related mortality risk, Honda et al. (2014) proposed Excessive Mortality Risk (EMR) by using an empirical relationship between daily maximum temperature (Tmax) and the daily number of deaths. He found a skewed V-shaped curve in the historical datasets from 47 Japanese regions, and defined the optimum temperature (OT) where the mortality becomes lowest as the 84th percentile value of daily Tmax, which was also valid in 32 cities across Asia, America, and Europe. Setting out the mortality risk at OT as a baseline of 1, the relative mortality risk against Tmax beyond OT increases along with the upward curve that shapes proportionally to the degree of difference between the OT and Tmax exceeding the OT, but in a nonlinear manner (see Section 2). Based on this, the ratio of accumulated EMR between future and historical periods can be interpreted as the potential impacts of temperature change on mortality. Such an empirical formula (Honda et al. 2014) that requires only the climate data as the input has an advantage for calculation. In fact, the empirical formula presented in Honda et al. (2014) applied to Africa and the Middle East in order to depict future risk of heat-related mortality (Ahmadalipour et al. 2019; Ahmadalipour and Moradkhani 2018) and also demonstrated the feasibility of global application (Fan et al. 2022). In particular, Fan et al. (2022) demonstrated that the gradient of empirical curve might have a marginal impact on the spatial distribution of heat-related mortality as long as it is monotonic increasing beyond OT. However, this insensitivity may continue to be questioned under much severe warming conditions and special curve curvatures of the association between Tmax and mortality. Therefore, it is necessary to investigate the global distribution of heat-related mortality based on the different shapes of empirical curves.

In this study, we attempt to estimate the robustness of the regional hotspots of heat-related mortality increase by examining its sensitivity to EMR relationships under the two contrary "representative concentration pathways" (RCPs): RCP2.6 and RCP8.5. Notably, both scenarios describe future trajectories of GHG emissions with entirely different mitigation strategies (Moss et al. 2010), which can enhance the contrast to the largest extent in our comparative assessment. The RCP8.5 corresponds to the so-called "business-as-usual" scenario with the highest GHG emissions, whereas the RCP2.6 represents strong mitigation ambition, which is roughly equivalent to 2 °C warming scenario pledged by the Paris Climate Agreement. A comparative analysis of heat-related mortality risk projected under the RCP2.6 and RCP8.5 scenarios will be able to quantify the benefit of mitigation. Possible future climate conditions that consider GHG concentrations from the different RCPs are obtained from a massive volume of fine-scale climate dataset that was recently completed within the Coordinated Regional Climate Downscaling Experiment-Coordinated Output for Regional Evaluation (CORDEX-CORE) project (Giorgi et al. 2022). While the dynamically downscaled dataset using regional climate models (RCM) has been acknowledged to demonstrate the added value to better elucidate the region-specific patterns of climate change (Im et al. 2020; Qiu and Im 2021; Torma et al. 2015), one of the critical draw-backs is that the downscaling results for different regions are highly heterogeneous in terms of the experimental design (e.g., resolution, driving forcing), thereby rendering it difficult to compare future climate behavior across multiple domains. CORDEX-CORE was initiated to address this issue; to that end, one of its objectives is to provide homogeneous and intra-comparable datasets of 21st-century climate projections (Giorgi et al. 2022). This study leverages this dataset across six different domains (i.e., Europe, Africa, South Asia, East Asia, Southeast Asia, and Australia, see Table 1), which will offer a unique opportunity for the comparative assessment of the regional disparity of global warming impact on heat-related mortality risk in a systematic manner. The empirical formulas to calculate EMR are obtained using the mortality and Tmax data from Japan, UK, and Korea (see Section 2). The systematic comparison of future changes in mortality risk derived from three different empirical formulas will reveal the potential and limitation to apply a single formula based on a particular location to global scales. In addition to the broad patterns of global distribution, in-depth analysis based on the changes in frequency and intensity of Tmax is performed focusing on several target regions in order to uncover the dominant factor controlling the projected mortality risk ratio. For simplicity, the abbreviations listed in Table 2 will be adopted in this paper.

2 Materials and Methods

Daily Tmax over a reference period (1986–2005) and a future period (2079–2098) was obtained from the CORDEX-CORE archive (Giorgi et al. 2022). While Regional Climate Model version 4 RegCM4 (Giorgi et al. 2012) was commonly used to downscale three different global climate models (GCMs), its version was rather different. The future time slice ends at 2098 since the incompleteness of data in 2099. Table 1 depicts the details of the modeling chain (GCM-RCM) across the six different domains (Giorgi et al. 2022; Ashfaq et al. 2020). With respect to individual domains, the sensitivity tests for optimization were conducted and the convective parameterization scheme exhibiting the best performance was selected (Giorgi et al. 2022). Three GCMs, namely the Norwegian Earth System Model NorESM1-M (Bentsen et al. 2013), the Max Planck Institute

Table 1 RegCM4 configuration over six CORDEX-CORE domains

Domain	Driving GCM	Resolution	RegCM version	Convective parameterization schemes
Europe (EUR)	NorESM1-M (NO) MPI-ESM-LR* (MP) HadGEM2-ES (HA)	12 km	RegCM4.6.1	Tidtke
Africa (AFR)	NorESM1-M (NO) MPI-ESM-MR (MP) HadGEM2-ES (HA)	25 km	RegCM4.7.0	Tidtke over land Kain-Fritsch over ocean
West and South Asia (WAS)	NorESM1-M (NO) MPI-ESM-MR (MP) MIROC5* (HA)	25 km	RegCM4.7.0	MIT-Emanuel over land Tidtke over ocean
East Asia (EAS)	NorESM1-M (NO) MPI-ESM-MR (MP) HadGEM2-ES (HA)	25 km	RegCM4.4.1	MIT-Emanuel
Southeast Asia (SEA)	NorESM1-M (NO) MPI-ESM-MR (MP) HadGEM2-ES (HA)	25 km	RegCM4.7.0	Tidtke
Australia (AUS)	NorESM1-M (NO) MPI-ESM-MR (MP) HadGEM2-ES (HA)	25 km	RegCM4.7.0	Tidtke

All domains adopt Sub-grid Explicit Moisture Scheme as the grid-scale cloud process scheme and CLM4.5 as the land surface model. * indicates different GCM from other domains, but it is treated with the same name for convenience

Table 2 Abbreviation list

Abbreviation	Explanation
RCP	Representative concentration pathways
GHG	Greenhouse gas
GCM	Global climate model
CORDEX-CORE	Coordinated Regional Climate Downscaling Experiment-Coordinated Output for Regional Evaluation
EQ	Equatorial region between 10 N and 10 S
non-EQ	Non-equatorial region outside 10 N and 10 S
ENS	Ensemble of three GCMs in CORDEX-CORE
ECMWF	European Centre for Medium-Range Weather Forecasts
ERA5	ECMWF atmospheric reanalysis dataset
HIST	Historical period that is used as a reference period (1986–2005)
FUT	Future period (2079–2098)
Tmax	Daily maximum temperature
OT	Optimum temperature, which is the 84% percentile of Tmax in HIST
ΔT	Temperature offset, ΔT = Tmax-OT
RMR	Relative mortality risk
RMR_JP	Relative mortality risk equation derived from Japan's dataset
RMR_UK	Relative mortality risk equation derived from UK's dataset
RMR_KR	Relative mortality risk equation derived from Korea's dataset
EMR	Excessive mortality risk
EMR_JP	Excessive mortality risk equation derived from Japan's dataset
EMR_UK	Excessive mortality risk equation derived from UK's dataset
EMR_KR	Excessive mortality risk equation derived from Korea's dataset
EMR ratio	EMR ratio between EMR in future and reference period
EMR_JP ratio	EMR ratio derived from RMR_JP
EMR_UK ratio	EMR ratio derived from RMR_UK
EMR_KR ratio	EMR ratio derived from RMR_KR

for Meteorology Earth System Model-Mixed Resolution MPI-ESM-MR (Stevens et al. 2013), and the Met Office Hadley Centre Earth System model HadGEM2-ES (Jones et al. 2011) were downscaled as these GCMs encompass a broad range of climate sensitivities to the anthropogenic forcing and have been shown to perform reasonably over the domains. However, there are two exceptions. First, HadGEM2-ES was substituted with the Model for Interdisciplinary Research on Climate MIROC5 (Watanabe et al. 2010) for the West and South Asia domain because it completely failed to capture the monsoonal rainband (Ashfaq et al. 2017). Second, instead of MPI-ESM-MR, MPI-ESM-LR was downscaled over the European domain with a higher resolution of 12 km which was produced under the EURO-CORDEX protocol (Jacob et al. 2020). For the sake of simplicity, three GCMs are hereafter referred to as NO (NorESM1-M for all domains), MP (MPI-ESM-LR for Europe, and MPI-ESM-MR for other domains), and HA (MIROC5 for South Asia and HadGEM2-ES for other domains). The fifth-generation ECMWF (European Centre for Medium-Range Weather Forecasts) atmospheric reanalysis dataset (hereafter referred to as ERA5) is used for the same period of reference simulation (1986–2005) to validate the Tmax data in CORDEX-CORE simulations. Although it may not perfectly capture all the regional details, it is still worth adopting ERA5 in a long-term and global-scale comparison (Parker 2016; Velikou et al. 2022; Hersbach et al. 2020). The maximum of hourly ERA5 data is regarded as the daily Tmax with resolution of 0.5 degree.

To assess the sensitivity of EMR to curve shape, three relative mortality risks (RMR) are calculated based on the same OT stipulation, which is defined as the 84th percentile of Tmax in this paper. RMR formulas presented in Eqs. (1), (2), and (3) are retrieved from the empirical curve of the relationship between relative mortality risk and temperature extracted from Japan's dataset (RMR_JP), UK's dataset (RMR_UK) and Korea's dataset (RMR_KR) at a daily time-scale (Kang et al. 2020). RMR_JP is formulated by previous studies (Honda et al. 2014; Ahmadalipour and Moradkhani 2018), while another two RMR curves are derived from daily Tmax and mortality in 10 stations in the United Kingdom (RMR_UK) during 1990–2012 (23 years) and 2 cities (i.e., Pusan and Seoul) in Korea (RMR_KR) during 1997–2020 (24 years). Exactly same process of RMR_JP employed by Honda (Honda et al. 2014) is performed to in the derivation of RMR_UK and RMR_KR to establish a fair comparison between equations, including the preprocess of death data normalization and function postulation by the distributed lag non-linear model with upto 15 days lag. The offset between Tmax and OT is denoted as $\Delta T = \text{Tmax-OT}$. Setting out the RMR as 1 at the OT (i.e., $\Delta T = 0$), the RMR increases as Tmax exceeds the OT.

$$Daily\ RMR\_KR = 1.44 \times 10^{-4}\Delta T^3 - 0.0061\Delta T^2 + 0.00744\Delta T + 1 \quad (1)$$

$$Daily\ RMR\_UK = 1.91 \times 10^{-5}\Delta T^3 + 0.00279\Delta T^2 + 0.00302\Delta T + 1 \quad (2)$$

$$Daily\ RMR\_JP = -2.91 \times 10^{-5}\Delta T^3 + 0.00153\Delta T^2 + 0.0054\Delta T + 1 \quad (3)$$

RMR_JP performs smooth growth up to about 18% risk increase within 10℃ Tmax offset (Fig. 1). With a more than 30% risk increase within 10℃ offset, RMR_UK presents steep convexity as expected since the UK, a high-latitude country, is supposed to be more sensitive to heat weather than Japan in the mid-latitude. On the other hand, RMR_KR shows rather concave, whose mortality gradually levels off with extreme heat intensifying. Although it has high values within the early and middle stages, it finally lags behind the more sensitive RMR_UK. This is likely caused by relatively scattered data distribution and the lag effect. This shape can represent those minor cases among regional heat-mortality relationships (Gasparrini et al. 2016; Kephart et al. 2021), evaluating the robustness of EMR in those regions. Compared with RMR_JP, RMR_UK outstrips especially with large offsets since its gradient keeps going steep, while RMR_KR overrates more in small to middle offset attributed to its bulge in the early stage. Since all three curves represent distinct growth trajectories that emphasize different Tmax offset ranges, it is important to quantify how the difference in empirical formula can translate into the calculation of heat-related mortality, particularly when calculating ratios between future and historical periods since Tmax distribution varies drastically with global warming.

When Tmax exceeds OT, all these RMR relationships (i.e., Daily RMR_UK, Daily RMR_KR, Daily RMR_JP, collectively named Daily RMR) are individually accumulated over 20 years in the target period (e.g., reference or future

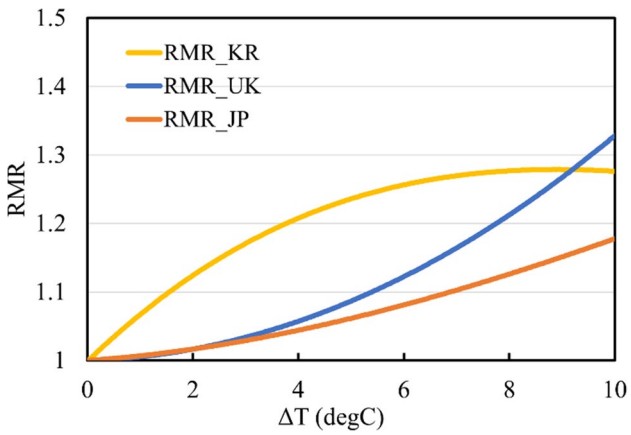

Fig. 1 Relative mortality risk as a function of Tmax offset in Korea, United Kingdom, and Japan

period), which is defined as the excessive mortality risk as presented in Eq. (4):

$$Daily\ EMR = Daily\ RMR - 1, if\ \Delta T > 0 \tag{4}$$

It is noteworthy that OT should remain consistent between the reference period and the future period, so the 84th percentile of Tmax from the reference period should also be considered as the OT in the future period. In other words, when calculating the EMR during the future period (2079–2098) forced by the RCP2.6 and RCP8.5 scenarios, the OT remains the same as the one calculated from the reference period. Based on the relative ratio of future EMR against reference EMR in Eq. (5), it is possible to estimate the potential increase in heat-related mortality risk that is solely attributed to higher Tmax under global warming. Since the calculation is done for each grid point, the OT implicitly reflects relative heat acclimatization across different regions. Although the percentile of defining OT may not be exactly uniform among all regions, the final result should not depend heavily on its selection (i.e., 84th) when studying the relative changes of heat-related mortality, which has been demonstrated in multiple climate zones (Honda et al. 2014; Ahmadalipour and Moradkhani 2018; Ahmadalipour et al. 2019; Fan et al. 2022; Christidis et al. 2019).

$$Relative\ Ratios = \frac{\sum Daily\ EMR\ in\ FUT}{\sum Daily\ EMR\ in\ HIST} \tag{5}$$

3 Results

3.1 Validation of Tmax from the CORDEX-CORE Simulations

We first investigate how the downscaled simulations across different domains can capture the geographical patterns and magnitude of OT. Figure 2a–b presents the spatial distribution of the OT calculated as the 84th percentile of Tmax during the historical period derived from the CORDEX-CORE simulations and ERA5 reanalysis data. For the simulations, the OT is calculated with respect to individual members (see Table 1), following which we take an ensemble of three members (hereafter referred to as ENS). Given that the study focuses on the heat mortality

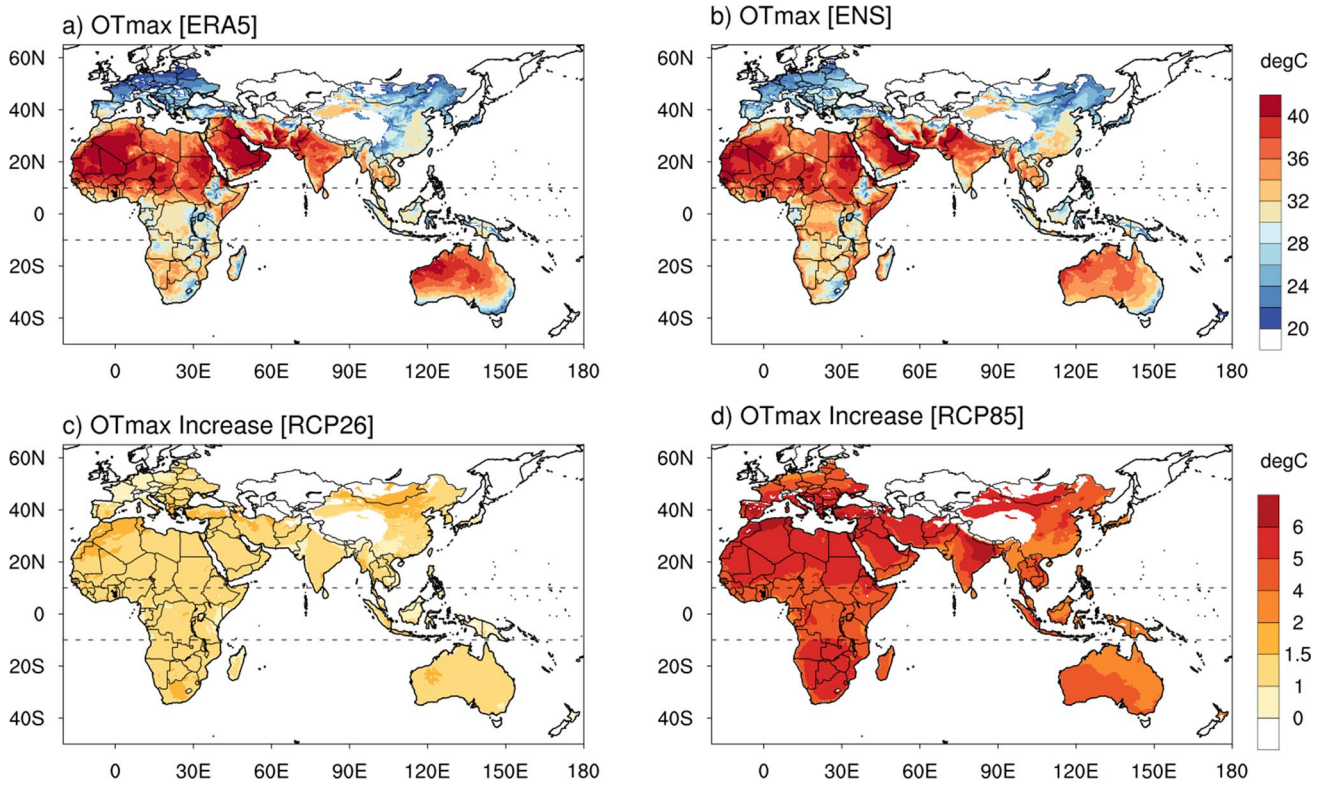

Fig. 2 Climatological mean of the 84th percentile of **a** Tmax derived from ERA5 reanalysis dataset; **b** Tmax derived from ensemble mean of downscaled simulations during the reference period (1986–2005). The gray dashed lines indicate the equatorial region between 10°N and 10°S. The regions where Tmax is below 20 °C are excluded from the analysis (no color shading). The changes in the 84th percentile of **c** Tmax under the RCP2.6; **d** Tmax under RCP8.5 scenarios against the reference simulation. The gray dashed lines indicate the equatorial region between 10°N and 10°S

caused by extremely high temperatures, areas with the OT less than 20℃ are excluded from the analysis. Even though some heat events also happen in these regions, the assessment may not be reasonable since the settlement of OT is so low that even a relatively mild temperature can cause a considerable Tmax offset leading to exponentially high risk. The threshold of 20℃ is arbitrarily selected, but as illustrated in Fig. 1, the masked areas are limited to high mountains (e.g., Himalayas) and some parts of northern Europe, which will not affect the general spatial distribution. Overall, the ENS shows a good performance in terms of capturing the geographical characteristics of OT, showing higher values over subtropical latitudes (e.g., northern Africa, Arabian Peninsula, India subcontinent and northern Australia). The strong similarity between ENS and ERA5 patterns yields a spatial correlation coefficient of 0.94 between them.

Additionally, the spatial distribution of changes in the 84th percentile of Tmax is presented in Fig. 2c–d. The difference of the 84th percentile of Tmax between the reference and future periods provides a clear picture of temperature response under the RCP2.6 and RCP8.5 scenarios, which will convey the mortality risk. As expected, the increase in temperature reflects a strong sensitivity to emission forcing. The 84th percentile of Tmax under the RCP8.5 scenario increases more than 4 °C in most of the regions against the reference period. On the other hand, the heightened temperature is mostly limited to less than 2 °C under the RCP2.6 scenario, thus suggesting strong mitigation effects. The increase in OT shows different patterns among different domains. Heat increase appears to be stronger in southern part of EUR, while in northern part of EAS, AUS, AFR and WAS, projecting a reverse direction of latitudinal deepening.

3.2 Projection of Mortality Risk Attributed to the Increase in Tmax

Figure 3 shows the mortality risk changes by plotting EMR ratios under the RCP2.6 and RCP8.5 scenarios using three empirical formulas, which roughly represent the ratio of heat-related excess deaths between the future and historical period. For future periods, it is obvious that the heat-related mortality risk will increase in almost all places, albeit with varying severity levels according to the emission scenarios. Under the RCP2.6 scenario where temperatures stabilize in the second half of the 21st century (Moss et al. 2010), the mortality risk is projected to increase mostly 4 times higher than that of the reference period with all equations, except for a few regions in Africa and Maritime Continent experiencing more than 5 times. More specifically, 4 times higher EMR can be obtained from the cases where either the heatwave occurrence becomes 4-fold frequent, or the average death of single-day heat is 4 times more due to the increased intensity of heatwave, or both are mixed. Meanwhile, the mortality risk rises sharply under the RCP8.5 scenario but with a similar spatial pattern to RCP2.6. The increasing ratio exceeds 20 times in comparison to the reference period in some places. More importantly, the regional hotspots with greater EMR emerge in the low latitudes, including Africa and Southeast Asia. These regions were also highlighted in other EMR studies (Ahmadalipour and Moradkhani 2018; Ahmadalipour et al. 2019; Fan et al. 2022), and reportedly experience the early emergence of a robust anthropogenic increase in heat stress using other evaluation indices (Im et al. 2020; King et al. 2015; Mahlstein et al. 2011). A notable vacancy with a relative lower risk ratio occurs in central African, which differs from Fan et al. (2022). The difference is foreseeable from the distinct OT increase pattern (Fig. 2d) inherently derived from datasets.

The variation derived from adopting curves with different heat sensitivity can be clearly seen in Fig. 3 under more intense global warming. Risk ratios of EMR_UK appear to be generally deeper with greater spatial dispersion due to the larger magnitude, but EMR_KR ratios are lighter with a more unified color distribution. This diversification can be explained by the curve convexity or concavity in Fig. 1. Compared with the smoothly growing RMR_JP, the exorbitant risk increases in the large offset range of RMR_UK leads to overestimation in the future period when Tmax becomes more likely to be extreme, while maintaining similar or slight changes in the historical period when most Tmax offset falls in the small offset range where RMR_UK doesn't differentiate much from RMR_JP. On the contrary, RMR_KR overvalues more significantly in the historical period, further producing smaller EMR ratios and more concentrated distribution along the equator since tropical region favors small offsets (more in Section 3.3). Although the magnitude and dispersion differences are noticeable, three curves perform unanimous outlines of heat-mortality risk increase, providing a robust base for regional hot-spots identification. Taken together, the dire impacts of global warming on heat-related mortality are quite foreseeable in the vast majority of regions of Africa and Southeast Asia especially those nestled within the equatorial region (10°N-10°S).

For a more quantitative measure of the heightened mortality risk, Fig. 4 illustrates the cumulative distribution of the extent of land exposure as a function of the increased mortality risk ratio. Besides the ranges formed by three different members, the ENS is denoted by the solid black lines, which shows a less fluctuating pattern when compared to a single individual model. In consonance with the former analysis, there is a clear right shift from RCP2.6 to RCP8.5 and from the non-equatorial region to the equatorial region. In the case of EMR_JP ratios from the ENS under the RCP2.6 scenario, a relatively small fraction of land (about 10%) from the non-equatorial region is projected to experience a mortality risk of more than 3 times than that in the reference

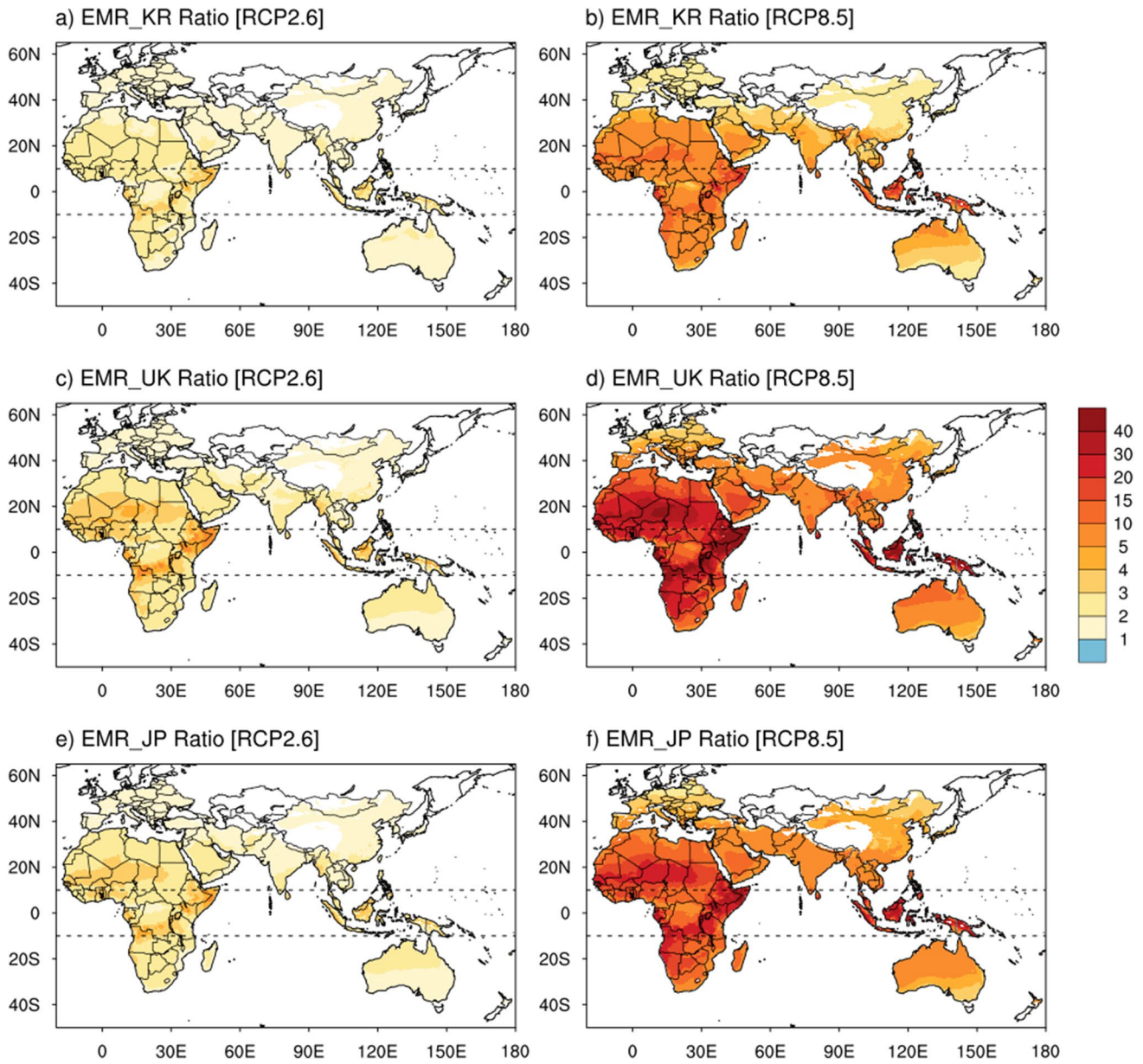

Fig. 3 Excessive mortality risk ratio between the reference period (1986–2005) and future period (2079–2098) calculated using **a**, **b** RMR_KR, **c**, **d** RMR_UK **e**, **f** RMR_JP under the **a**, **c**, **e** RCP2.6 and **b**, **d**, **f** RCP8.5. The gray dash line delineates equatorial region between 10°N and 10°S

period. However, a larger area of land from the equatorial region (about 43%) reaches this threshold. A similar situation transpires under the RCP8.5 scenario. While no part of the non-equatorial region will experience the increased mortality risk of more than 30 times, approximately 15% of the equatorial land will be exposed to that risky climate. Far more dramatic right shifts from non-equatorial to equatorial can be found with EMR_UK who overrates high offset generated in RCP8.5, where 9% versus 40% of land confronts a more than 30 times higher mortality risk than the reference period under RCP8.5 in equatorial and non-equatorial regions. The difference in the mortality risk projected for RCP8.5 and RCP2.6 suggests the demonstrable benefit that can be expected from substantial mitigation. The sensitivity of EMR ratios to the curve shapes also coincides with the overestimation of EMR_UK and underestimation of EMR_KR referring to EMR_JP. Under RCP8.5, the equatorial curve of EMR_JP ratio reaches 100% land cover at about 40 times, while EMR_UK extends to later than 50 times and EMR_KR even earlier than 30 times. Similarly, all lands are covered with about 30 times EMR_JP in non-equatorial region, while around 40 times and 20 times for

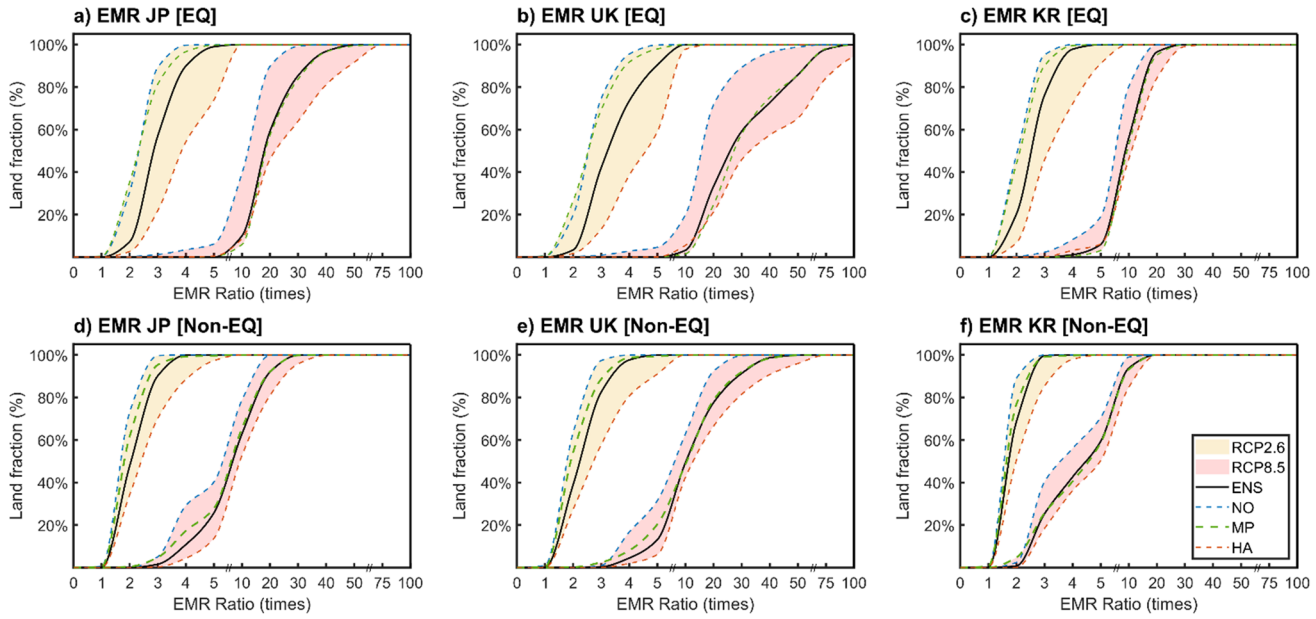

Fig. 4 Cumulative distribution of land area fractions (%) along the excessive RMR ratio for **a**, **b**, **c** equatorial region (10°S-10°N) and **d**, **e**, **f**) non-equatorial region derived from **a**, **d** EMR_JP **b**, **e** EMR_UK and **c**, **f** EMR_KR.

EMR_UK and EMR_KR, respectively. Moreover, the line ranks from left to right are NO, HA, and MP in most cases, which are exactly the same as the warming sensitivity order to greenhouse gas forcings (Giorgi et al. 2022; Im et al. 2020). However, the sensitivity of a model may not always be the same in both low-risk and high-risk areas, which leads to an intersection in Fig. 4b. And the shading area is wider in EMR_UK among all three formulas and in equatorial region compared with non-equatorial region, revealing higher ensemble disconformity exists in low latitudes and with EMR_UK, possibly induced by higher values of EMR ratios.

3.3 Analysis of EMR Ratio in Response to Changes in Intensity and Frequency of Tmax

To uncover the controlling factor of heat-mortality increase and its consistent spatial pattern regardless of curve sensitivity, at least two regions enclosing the deepest and lightest color are selected from each CORDEX-CORE domain (see Table 1). For those domains sitting astride the equatorial and non-equatorial area (i.e., AFR and SEA), two boxes are deliberately designated from each region. An extra box is added in AFR to better analyze the deficiency in central Africa. For consistency, boxes are ordered by the mean risk ratios in each domain. Figure 5 depicts frequency distributions of Tmax offset in historical period and in future RCP8.5 period. Relevant distributions from the same box are tinted with the same color but different transparency (i.e. solid blue for historical distribution of Region1 and translucent blue for RCP8.5 distribution of Region1). The definition of OT as 84th percentile of historical dataset determines that the height summation of each solid color must be 16%, forming a fair comparison between regions. But the integral area of future distribution differs from domain to domain. As expected, SEA displays the highest risk ratio, followed by AFR, while EUR generally displays the lowest and the smallest rises but striking high values with Tmax offset greater than 10 among all domains under RCP8.5 scenario. In general, non-equatorial area has a wider distribution of temperature offset than equatorial area due to higher climate variability.

Moreover, in AUS, Region 2 dominates Region 1 within the small Tmax offset range, which should be the major reason that Region 2 has higher risk ratios. But Region 1 gradually surpasses Region 2 when reaching a greater offset in both historical and RCP8.5 periods. Surprisingly, this tendency can also be found in SEA, EAS, WAS regardless of period. A potential explanation would be, Region 2, located closer to the tropical climate, has an inherently low variability in temperature. As a result, Tmax fluctuates around the OT thresh line, frequently hits but does not exceed appreciably beyond, forming a heavy head. With global warming, it is easy to have an incomparable sharp frequency increase in these stable climates (e.g., in SEA), finally leads to high EMR ratios. Also, limited by its invariability, Tmax in Region2 can hardly rush to an extremely high value, gradually lags behind Region1 when it comes to larger offsets. But the relatively minor rise in the high-offset range in Region1 cannot catch up with the predominant low-frequency escalations in Region2. In other words, the stable tropical climate favors overriding

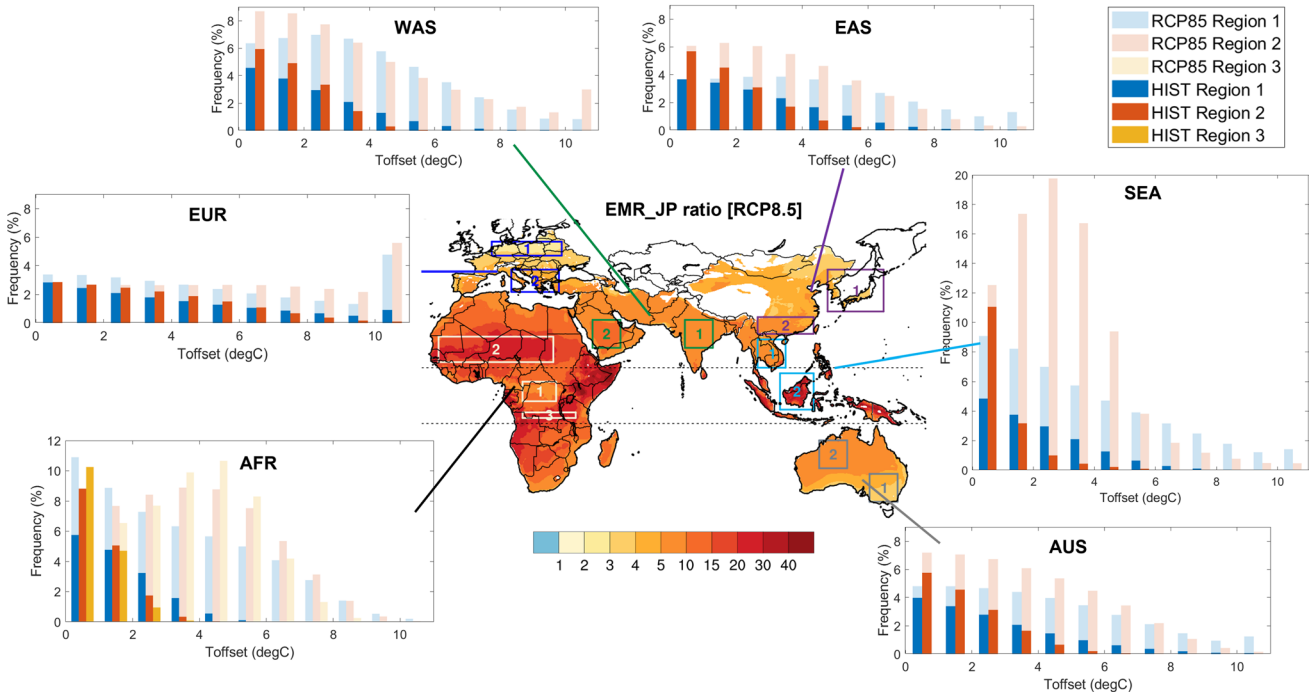

Fig. 5 Frequency distribution of Tmax offset over different regions in the historical period (solid colors) and future RCP8.5 period (translucent colors). The locations of regions are delineated on the EMR_JP ratio map under RCP8.5 (same as Fig. 3f). The gray dash line delineates the equatorial region between 10 N and 10 S

surges in slight but frequent heat and finally contributes more to the heat-mortality risk increase, which confirms the leading role of frequency in the heat-related mortality increase concluded in other studies (Ahmadalipour et al. 2019; Fan et al. 2022).

But this inclination is not irrefutable. In EUR and AFR, although the distribution of Region2 (or Region3 in AFR) appears to be heavy-headed in the historical period, it is distorted, even transformed reversely into a heavy-tailed shape. The considerable growth amount in the middle or latter part supplies enough support for Region2 to have a greater risk ratio increase than Region1, which is also the reason for the central Africa loophole. the particularity in EUR from other four domains is also indicated earlier in the OT increase map (Fig. 2c–d) when EUR is the only domain containing an inverse meridional pattern. Thus, both frequency-dependent background climate and global-warming-induced variation determine the spatial disparity of heat-related mortality risk elevation jointly.

4 Discussion

This study examines the spatial distribution of potential increase in heat-related mortality risk due to GHG-induced anthropogenic warming as well as its sensitivity to the adoption of different empirical formulas between temperature and mortality. The future climates in response to very different radiative forcing pathways (RCP2.6 vs. RCP8.5) are realized using a well-organized climate modeling framework, so-called CORDEX-CORE (Giorgi et al. 2022). Although the implausibility of RCP8.5 has been put forward (Hausfather and Peters 2020), it's still common and worthy to adopt RCP8.5 in the heat-related studies, in order to amplify the climate response and discern the future trend (Ho et al. 2021; Choi and Lee 2019; Im et al. 2017). A systematic comparison of relative changes across the six different domains makes it possible to identify more vulnerable regional spots in terms of heat-related mortality in tandem with global warming. Despite the presence of an overwhelming consensus that accelerating global warming will escalate the health burden of hot temperatures, the direct correlation between ambient temperature and mortality remains obscure because it varies on the basis of many other climates (e.g., humidity, wind) and socioeconomic (e.g., demography, public health system) factors. For instance, it is widely accepted that the moisture level can largely influence a human's perception of high temperature (Anderson et al. 2013; Steinweg and Gutowski 2015), and therefore, wet-bulb temperature comprising both temperature and relative humidity is popularly adopted in heat stress studies (Sherwood and Huber 2010; Sherwood 2018). However, the empirical relationship

derived from wet-bulb temperature (or other heat stress indices) and mortality has rarely been reported. Besides the variation in temperature and mortality association, the reliability of future assessment of heat-related mortality is contingent on the quality of future climate information. The majority of previous studies that have projected heat-related mortality were based on either global climate projections with coarse resolution or downscaled results with higher resolution but over a limited target region. In particular, it may not be common to use the dynamically downscaled results across multiple domains. In this regard, the study can take advantage of the CORDEX-CORE dataset that provides a homogeneous set of fine-scale long-term projections over multiple domains at multi-continental scales (Giorgi et al. 2022).

This study adopts the simplified concept of a skewed V-shaped curve put forward by Honda et al. (2014) based on the empirical relationship of daily data between the number of deaths and Tmax. The mortality risk increases followed by the OT at which the mortality is at the minimum. Therefore, as the temperature is distanced far from the OT, the excessive mortality risk can gradually increase. While there is no single formula to determine the OT and temperature-mortality risk curve, the present study assigns the OT as the 84th percentile value of Tmax from the historical data with respect to individual locations, which is consistent with the previous research such as Honda et al. (2014), Ahmadalipour & Moradkhani (2018), Ahmadalipour et al. (2019) and Fan et al. (2022). The OT determined by the region-specific climatology is capable of implicitly accounting for varying levels of heat acclimatization. The OT for each grid is then used for quantifying the increase in the excessive mortality risk in a warmer future climate expected from the RCP2.6 and RCP8.5 emission pathways. It is important to note that the temperature and mortality association and the OT would remain unchanged in the course of future warming. Even though we choose three curves with diverse curvatures, this study cannot fully consider all modes of relationships found by other station-based studies (Gasparrini et al. 2016; Vicedo-Cabrera et al. 2021; Kephart et al. 2021). Especially, those three curves extracted from mid to high-latitude countries may not fully represent the relationship in equatorial, which usually have a flatter curve representing its lower sensitivity to heat stress (Kephart et al. 2021; Vicedo-Cabrera et al. 2021; Lin et al. 2019). Although the uncertainty cannot be eliminated, the application of EMR ratio can somehow reduce the systematic overestimation or underestimation, and a previous paper (Fan et al. 2022) also claimed that the gradient of EMR equations caused an insignificant deviation in the EMR ratio. In addition, socioeconomic factors that critically affect heat-related mortality are not included in the assessment. For instance, the population growth and the age structure are expected to change over time and across regions, and not considering such factors can lead to a distorted quantitative assessment of mortality risk (Fan et al. 2022; Park et al. 2020; Chen et al. 2020). While we duly acknowledge all these limitations, the objective of this study is to quantify the "relative" changes in heat-related mortality risk solely attributed to higher Tmax. To that end, a strong focus is directed on the comparative assessment of future risk under the RCP2.6 and RCP8.5 emission scenarios, thus emphasizing the necessity of mitigating climate change. The ensembles of dynamically downscaled projections clearly reveal that the risk level of heat-related mortality will greatly depend on the future GHG emission scenarios. While the increase in heat-related mortality risk response to RCP2.6 will be confined to less than 5 times over the vast majority of regions, the Tmax projected from RCP8.5 could result in the emergence of highly vulnerable regions with more than 20 times higher mortality risk against the historical period. The massive land area fraught with the highest increase of mortality risk appears in the African continent and Southeast Asia regions with limited capacity to adapt and to manage the extreme heat (Intergovernmental Panel on Climate Change 2014; Im et al. 2018). By making a comparison with the land fraction along with the increased ratio of mortality risk between the equatorial and non-equatorial regions, the regions experiencing a higher risk of mortality are aggressively expanded in the low-latitude, whereas the increase in mortality risk appears to stagnate outside the equator. This behavior becomes much clearer under RCP8.5 than under RCP2.6. Although some differences are found in the regional details of the mortality risk derived from different heat formulas, the large vulnerability to the low-latitude areas near the equator is common. Considering the methodological limitation addressed above, the findings of our study must not be viewed as the prediction of the future excess mortality, but rather be interpreted as potential impacts of higher temperature on mortality that may significantly vary along the future emission pathways. Nevertheless, the drastic difference in mortality risk expected from RCP2.6 and RCP8.5 would have significant implications for not only initiating immediate mitigation policies but also preparing better adaptation strategies.

Acknowledgements This research was supported by the Faculty Initiation Grant (IGN16EG02) funded by The Hong Kong University of Science and Technology (HKUST). This study was also partly carried out with the support of "Research Program for Agricultural Science & Technology Development (Project No. PJ014882)," National Institute of Agricultural Sciences, Rural Development Administration, South Korea. We would thank Dr. Shin Ju-Young and Dr. Kyu Rang Kim who shared the mortality data in Korea with us.

Data Availability The CORDEX-CORE data used in this work can be found at the Earth System Grid Federation (ESGF) databanks following the CORDEX output specifications. The code and script used for analysis are available from the corresponding author upon reasonable request.

Declarations

Conflict of Interest The authors declare no conflict of interest. The funders had no role in the design of the study; in the collection, analyses, or interpretation of data; in the writing of the manuscript, or in the decision to publish the results.

References

Ahmadalipour, A., Moradkhani, H.: Escalating heat-stress mortality risk due to global warming in the Middle East and North Africa (MENA). Environ. Int **117**, 215–225 (2018). https://doi.org/10.1016/j.envint.2018.05.014

Ahmadalipour, A., Kumar, M.: Mortality risk from heat stress expected to hit poorest nations the hardest. Clim. Change **152**, 569–579 (2019). https://doi.org/10.1007/s10584-018-2348-2

Anderson, G.B., Bell, M.L.: Heat waves in the United States: mortality risk during heat waves and Effect Modification by Heat Wave characteristics in 43 U.S. Communities. Environ. Health Perspect **119**, 210–218 (2011). https://doi.org/10.1289/ehp.1002313

Anderson, G.B., Peng, R.D.: Methods to calculate the Heat Index as an exposure Metric in Environmental Health Research. Environ. Health Perspect **121**, 1111–1119 (2013). https://doi.org/10.1289/ehp.1206273

Ashfaq, M., Rastogi, D., Mei, R., Touma, D., Ruby Leung, L.: Sources of errors in the simulation of south asian summer monsoon in the CMIP5 GCMs. Clim. Dyn **49**, 193–223 (2017). https://doi.org/10.1007/s00382-016-3337-7

Ashfaq, M., et al.: Robust late twenty-first century shift in the regional monsoons in RegCM-CORDEX simulations. Clim. Dyn (2020). https://doi.org/10.1007/s00382-020-05306-2

Bentsen, M., et al.: The norwegian Earth System Model, NorESM1-M – part 1: description and basic evaluation of the physical climate. Geosci. Model. Dev **6**, 687–720 (2013). https://doi.org/10.5194/gmd-6-687-2013

Chen, J., et al.: Global socioeconomic exposure of heat extremes under climate change. J. Clean. Prod **277**, 123275 (2020). https://doi.org/10.1016/j.jclepro.2020.123275

Chen, R., et al.: Association between ambient temperature and mortality risk and burden: time series study in 272 main chinese cities. BMJ. k4306 (2018). https://doi.org/10.1136/bmj.k4306

Choi, N., Lee, M.-I.: Spatial variability and long-term trend in the occurrence frequency of heatwave and tropical night in Korea. Asia-Pac. J. Atmos. Sci **55**, 101–114 (2019)

Christidis, N., Mitchell, D., Stott, P.A.: Anthropogenic climate change and heat effects on health. Int. J. Climatol **39**, 4751–4768 (2019). https://doi.org/10.1002/joc.6104

Fan, Y., Liao, P.-S., Im, E.-S., Lo, M.-H.: Regional disparities in the exposure to heat-related mortality risk under 1.5°C and 2°C global warming. Environ. Res. Lett (2022). https://doi.org/10.1088/1748-9326/ac5adf

Gasparrini, A., et al.: Changes in susceptibility to Heat during the summer: a Multicountry Analysis. Am. J. Epidemiol **183**, 1027–1036 (2016). https://doi.org/10.1093/aje/kwv260

Giorgi, F., et al.: RegCM4: model description and preliminary tests over multiple CORDEX domains. Clim. Res **52**, 7–29 (2012). https://doi.org/10.3354/cr01018

Giorgi, F., et al.: The CORDEX-CORE EXP-I Initiative: description and highlight results from the initial analysis. Bull. Am. Meteorol. Soc **103**, E293–E310 (2022). https://doi.org/10.1175/BAMS-D-21-0119.1

Guo, Y., et al.: Quantifying excess deaths related to heatwaves under climate change scenarios: a multicountry time series modelling study. PLoS Med **15**, e1002629 (2018). https://doi.org/10.1371/journal.pmed.1002629

Hausfather, Z., Peters, G.P.: Emissions – the 'business as usual' story is misleading. Nature **577**, 618–620 (2020). https://doi.org/10.1038/d41586-020-00177-3

Hersbach, H., et al.: The ERA5 global reanalysis. Q. J. R Meteorol. Soc **146**, 1999–2049 (2020). https://doi.org/10.1002/qj.3803

Ho, C.-H., Park, C.-K., Yun, J., Lee, E.-J., Kim, J., Yoo, H.-D.: Asymmetric expansion of summer season on May and September in Korea. Asia-Pacific J. Atmos. Sci **57**, 619–627 (2021). https://doi.org/10.1007/s13143-020-00220-3

Honda, Y., et al.: Heat-related mortality risk model for climate change impact projection. Environ. Health Prev. Med **19**, 56–63 (2014). https://doi.org/10.1007/s12199-013-0354-6

Im, E.-S., Pal, J.S., Eltahir, E.A.B.: Deadly heat waves projected in the densely populated agricultural regions of South Asia. Sci. Adv **3**, e1603322 (2017). https://doi.org/10.1126/sciadv.1603322

Im, E.-S., Kang, S., Eltahir, E.A.B.: Projections of rising heat stress over the western Maritime Continent from dynamically downscaled climate simulations. Glob. Planet Change **165**, 160–172 (2018). https://doi.org/10.1016/j.gloplacha.2018.02.014

Im, E.-S., Thanh, N.-X., Kim, Y.-H., Ahn, J.-B.: 2018 summer extreme temperatures in South Korea and their intensification under 3° C global warming. Environ. Res. Lett **14**, 094020 (2019)

Im, E.-S.: Emergence of robust anthropogenic increase of heat stress-related variables projected from CORDEX-CORE climate simulations. Clim. Dyn (2020). https://doi.org/10.1007/s00382-020-05398-w

Intergovernmental Panel on Climate Change: Managing the Risks of Extreme Events and Disasters to Advance Climate Change Adaptation: Special Report of the Intergovernmental Panel on Climate Change, p. 593. Cambridge University Press (2012)

Intergovernmental Panel on Climate Change: Climate Change 2013 - The Physical Science Basis: Working Group I Contribution to the Fifth Assessment Report of the Intergovernmental Panel on Climate Change. Cambridge University Press (2014)

Jacob, D., et al.: Regional climate downscaling over Europe: perspectives from the EURO-CORDEX community. Reg. Environ. Change **20**, 51 (2020). https://doi.org/10.1007/s10113-020-01606-9

Jones, C.D., et al.: The HadGEM2-ES implementation of CMIP5 centennial simulations. Geosci. Model. Dev **4**, 543–570 (2011). https://doi.org/10.5194/gmd-4-543-2011

Kang, M., Kim, K.R., Shin, J.-Y.: IJERPH. **17**, 2631 (2020). https://doi.org/10.3390/ijerph17082631 Event-Based Heat-Related Risk Assessment Model for South Korea Using Maximum Perceived Temperature, Wet-Bulb Globe Temperature, and Air Temperature Data

Kephart, J.L., et al.: *Extreme temperatures and mortality in 326 Latin American cities*. Epidemiology (2021)

King, A.D., et al.: The timing of anthropogenic emergence in simulated climate extremes. Environ. Res. Lett **10**, 094015 (2015). https://doi.org/10.1088/1748-9326/10/9/094015

Lin, Y.-K., Maharani, A.T., Chang, F.-T., Wang, Y.-C.: Mortality and morbidity associated with ambient temperatures in Taiwan. Sci. Total Environ **651**, 210–217 (2019). https://doi.org/10.1016/j.scitotenv.2018.09.161

Mahlstein, I., Knutti, R., Solomon, S., Portmann, R.W.: Early onset of significant local warming in low latitude countries. Environ. Res. Lett **6**, 034009 (2011). https://doi.org/10.1088/1748-9326/6/3/034009

Moss, R.H., et al.: The next generation of scenarios for climate change research and assessment. Nature **463**, 747–756 (2010). https://doi.org/10.1038/nature08823

Park, C.-E., Jeong, S., Harrington, L.J., Lee, M.-I., Zheng, C.: Population ageing determines changes in heat vulnerability to future warming. Environ. Res. Lett **15**, 114043 (2020). https://doi.org/10.1088/1748-9326/abbd60

Parker, W.S.: Reanalyses and observations: what's the difference? Bull. Am. Meteorol. Soc **97**, 1565–1572 (2016). https://doi.org/10.1175/BAMS-D-14-00226.1

Qiu, L., Im, E.-S.: Added value of high-resolution climate projections over South Korea on the scaling of precipitation with temperature. Environ. Res. Lett **16**, 124034 (2021). https://doi.org/10.1088/1748-9326/ac37d3

Saeed, F., Schleussner, C., Ashfaq, M.: Deadly heat stress to become Commonplace Across South Asia already at 1.5°C of global warming. Geophys. Res. Lett. **48** (2021). https://doi.org/10.1029/2020GL091191

Sherwood, S.C.: How important is humidity in heat stress? J. Geophys. Res. Atmos. **123** (2018). https://doi.org/10.1029/2018JD028969

Sherwood, S.C., Huber, M.: An adaptability limit to climate change due to heat stress. Proc. Natl. Acad. Sci. **107**, 9552–9555 (2010). https://doi.org/10.1073/pnas.0913352107

Steinweg, C., Gutowski, W.J.: Projected changes in Greater St. Louis summer heat stress in NARCCAP simulations. Weather Clim. Soc **7**, 159–168 (2015). https://doi.org/10.1175/WCAS-D-14-00041.1

Stevens, B., et al.: Atmospheric component of the MPI-M Earth System Model: ECHAM6. J. Adv. Model. Earth Syst **5**, 146–172 (2013). https://doi.org/10.1002/jame.20015

Sylla, M.B., Faye, A., Giorgi, F., Diedhiou, A., Kunstmann, H.: Projected heat stress under 1.5°C and 2°C global warming scenarios creates unprecedented discomfort for humans in West Africa. Earth's Future **6**, 1029–1044 (2018). https://doi.org/10.1029/2018EF000873

Torma, C., Giorgi, F., Coppola, E.: Added value of regional climate modeling over areas characterized by complex terrain-precipitation over the Alps: Added value of RCM over complex terrain. J. Geophys. Res. Atmos **120**, 3957–3972 (2015). https://doi.org/10.1002/2014JD022781

Velikou, K., Lazoglou, G., Tolika, K., Anagnostopoulou, C.: Reliability of the ERA5 in replicating Mean and Extreme Temperatures across Europe. Water **14**, 543 (2022). https://doi.org/10.3390/w14040543

Vicedo-Cabrera, A.M., et al.: The burden of heat-related mortality attributable to recent human-induced climate change. Nat. Clim. Chang **11**, 492–500 (2021). https://doi.org/10.1038/s41558-021-01058-x

Vogel, M.M., Zscheischler, J., Wartenburger, R., Dee, D., Seneviratne, S.I.: Concurrent 2018 hot Extremes Across Northern Hemisphere due to Human-Induced Climate Change. Earth's Future **7**, 692–703 (2019). https://doi.org/10.1029/2019EF001189

Watanabe, M., et al.: Improved climate simulation by MIROC5: Mean states, variability, and climate sensitivity. J. Clim **23**, 6312–6335 (2010). https://doi.org/10.1175/2010JCLI3679.1